Equivalent single layer and layerwise models for flutter and buckling analysis of supersonic variable stiffness laminated composite plates

Thin-Walled Structures 191 (2023) 111012

Contents lists available at ScienceDirect

Thin-Walled Structures

journal homepage: www.elsevier.com/locate/tws

Full length article

Equivalent single layer and layerwise models for flutter and buckling analysis of supersonic variable stiffness laminated composite plates

J.A. Moreira [a,*], F. Moleiro [a], A.L. Araújo [a], A. Pagani [b]

[a] IDMEC, Instituto Superior Tecnico, Universidade de Lisboa, Av. Rovisco Pais 1, Lisboa, 1049-001, Portugal
[b] MUL2, Department of Mechanical and Aerospace Engineering, Politecnico di Torino, Corso Duca degli Abruzzi 24, Torino, 10129, Italy

ARTICLE INFO

Keywords:
Panel flutter
Buckling
Variable stiffness composites
Layerwise theory
Equivalent single layer theory

ABSTRACT

This work provides an assessment of Equivalent Single Layer (ESL) and Layerwise finite element models, aimed for panel flutter and buckling analysis of supersonic variable stiffness composites, exploring variable-order shear deformation theories and Lagrange z-expansions. Numerical applications focus on simply supported panels with curvilinear fibre composite layers, including a cross-ply configuration for comparison purposes, and various side-to-thickness ratios. The accurate prediction of transverse shear and bending–twisting coupling is highlighted, as rather necessary for proper tailoring and analysis of supersonic curvilinear composites, especially when including in-plane loads. This is attainable through high-order ESL descriptions, in thin panels, even without thickness stretching.

1. Introduction

The ever-growing research on variable stiffness composite (VSC) laminates, involving curvilinear fibres technology, has consistently highlighted the exceptional tailor-ability and consequent superior structural efficiency in both strength and mass that can be attained by resorting to composite layers having carefully tailored curvilinear fibre paths [1]. In fact, among various cutting-edge engineering applications, the variable stiffness technology emerges quite suitable to be explored in the design optimization of advanced aerospace structures, either for improved buckling response [2–4], enhanced aeroelastic behaviour of wings [5–7] or increased supersonic panel flutter resistance [8–10]. Nonetheless, the accurate modelling of such highly anisotropic composite structures in terms of in-plane and transverse responses, including elastic coupling effects such as bending–twisting, is considered of the utmost importance for proper tailoring and analysis of curvilinear fibre composite laminates, especially when dealing with the combined effect of in-plane mechanical loads and transverse aerodynamic loads. In light of the challenging demands posed to the modelling of multilayered composite structures with curvilinear fibre paths, for which there is still a limited number of available literature discussing the role of structural theories on aeroelastic and buckling stability analysis, this work presents an assessment of kinematically refined finite element (FE) models, with either Equivalent Single Layer (ESL) or Layerwise (LW) descriptions, for panel flutter and buckling analysis of curvilinear fibre laminates under supersonic airflow and in-plane loading, pushing forward the structural modelling predictive capabilities to properly capture intricate effects that may be exhibited, with high numerical accuracy, all along ensuring computational efficient techniques.

The accurate analysis of multilayered composite structures, *per se*, relies mostly on the assumed structural theory and its capability to fully describe the displacements and stresses at the layer level, even if there is a high inhomogeneity of material properties between layers [11,12]. By adopting displacement based LW formulations, the necessary interlaminar continuity of displacements, shown by three-dimensional (3D) elasticity [13], can be fulfilled *a priori*, while allowing the prediction of zig-zag distributions along the thickness, as opposed to ESL descriptions. Further structural refinements are addressed, as appropriate, by high-order kinematic theories capable of rendering quasi-3D predictive capabilities in terms of in-plane response, transverse shear deformations and thickness stretching, especially when dealing with moderately thick and thick plates, as well as pronounced elastic coupling effects. It is relevant to point out that shear deformation plate theories, namely the First-order Shear Deformation Theory (FSDT) and Third-order Shear Deformation Theory (TSDT), focus solely on the kinematic enrichment of the in-plane displacements (maintaining a constant transverse displacement) and usually assume plane stress constitutive equations. General high-order thickness-expansions, in contrast, can act on all displacement components and, therefore, account for both transverse shear deformations and thickness stretching, while making use of the complete 3D constitutive equations.

As far as the analysis of curvilinear fibre composites is considered, some recent works on the application of refined structural models are indeed worth of mentioning. Actually, most of these investigations

* Corresponding author.
E-mail address: joao.anjos.moreira@tecnico.ulisboa.pt (J.A. Moreira).

https://doi.org/10.1016/j.tws.2023.111012
Received 27 April 2023; Received in revised form 3 July 2023; Accepted 8 July 2023
Available online xxxx

on the accuracy assessment of different models predictive capabilities are usually carried out resorting to unified formulations, such as the Carrera Unified Formulation (CUF) or the Generalized Unified Formulation (GUF), due to the sole purpose of encompassing various structural theories in a systematic and hierarchical fashion. In terms of static analysis of plates, Demasi et al. [14] applied the GUF to investigate ESL and LW descriptions, with various thickness-expansion orders of displacements. Likewise, Sánchez-Majano et al. [15] focused on the assessment of ESL and LW bi-dimensional (2D) CUF models for stress analysis of both plates and shells. Regarding the free vibration analysis of beams and plates, Viglietti et al. [16] provides an assessment of one-dimensional (1D) CUF models, which is further extended by Yan et al. [17] considering hierarchical differential quadrature finite elements with improved Legendre type expansions. Moreover, the application of variable-kinematic Ritz models, within the CUF framework, for free vibration and buckling analysis of variable stiffness composites are discussed by Vescovini and Dozio [18]. Additionally, the sensitivity analysis of the buckling and failure responses to manufacturing defects and fibre misalignments is also quite relevant in the design of curvilinear fibre composites, as highlighted in recent works by Sánchez-Majano et al. [19] as well as by Pagani and Sánchez-Majano [20,21], for which refined CUF models can ensure accurate global–local predictive capabilities. Aside from the widely used CUF, but still on the basis of the high-order LW modelling, Moreira et al. [22] implemented user-defined elements in the commercial software Abaqus for static and free vibration analysis of curvilinear fibre composite laminates, making use of the FSDT and TSDT displacement fields for each discrete layer. It is also worth mentioning other recent works on multi-walled carbon nanotube reinforced sandwich panels [23], delamination of composite plates and soft core sandwich shells [24,25] and functionally graded nanoshells [26].

However, in the supersonic panel flutter analysis of either straight or curvilinear fibre composites, the structural models tend to be simpler in order to achieve computationally bearable dynamic systems with reduced dimensions. As a matter of fact, the computational efficiency in general aeroelastic models is mostly demanded by the iterative nature of the flutter analyses, which require multiple eigenvalue extractions. Hence, the Rayleigh–Ritz method combining the Classical Laminated Plate Theory (CLPT) or the FSDT, and the First-order Piston Theory, as structural and fluid models, respectively, has been extensively used for panel flutter analysis [27], including aero-thermo-elastic stability and even active flutter and buckling control [28–31]. Further extensions to variable stiffness configurations are presented in the design optimization work by Guimarães et al. [8], highlighting remarkable improvements in flutter and buckling resistance via tailored curvilinear fibres, and by Moreira et al. [32] focusing on panel flutter of purely elastic laminates and active aeroelastic control in smart piezoelectric composites. Despite the assumption of no shear deformation in classical plate theories, it is relevant to note that since the most commonly used expansion functions in these Rayleigh–Ritz models are sinusoidal, which limits the analysis to simply supported plates, there is an additional overestimation of the stiffness in highly anisotropic composite laminates, involving elastic coupling effects such as bending–twisting coupling in the case of flexural anisotropy, as shown by Stone and Chandler [33] and Vescovini et al. [34]. In recent works by Sciascia et al. [35,36] on the vibration response and dynamic stability of pre-stressed variable stiffness composite shells, it is considered Legendre polynomials as Ritz expansion functions, showing a good agreement with standard FE models, including multi-part modelling of aerospace structures. Overcoming the underlying limitations of global Rayleigh–Ritz formulations, FE analyses of supersonic curvilinear fibre composites are reported by Akhavan and Ribeiro [37,38] through a p-version element which adopts Reddy's TSDT. In addition, Rasool and Singha [39] focused on the panel flutter response behaviour of pre-stressed curvilinear fibre composites using the FSDT. Still, these works just make use of ESL descriptions and shear deformation theories – which are not capable of predicting through-thickness zig-zag displacements and transverse normal strains nor use 3D constitutive equations – and do not present any comparative assessment between different structural models. Furthermore, it is worth remarking that Carrera and Zappino [40] and Zappino et al. [41] performed panel flutter analysis of supersonic pinched shells – representing the thermal insulation panels used in launcher structures – applying various structural models within CUF framework, as well as 1D and 2D type finite elements, respectively, though not including any variable stiffness configuration. Just recently, Yan and Zhang [42] extended 1D CUF models for aero-thermo-elastic stability analysis of curvilinear fibre composite laminates, assuming improved Legendre type expansion for the cross-section, which are able to predict, at most, quadratic through-thickness distributions of displacements in a LW sense. It is thus clear the limited number of available literature on the assessment of refined structural models for panel flutter and buckling analysis of supersonic composite laminates under in-plane loads, especially when the emerging and highly promising curvilinear fibre composites are considered.

To further extend the current knowledge on the role of structural theories in panel flutter and buckling stability analysis of supersonic composite laminates with curvilinear fibre paths, this work presents a comprehensive evaluation of various ESL and LW descriptions, considering either variable order shear deformation theories (i.e. Taylor z-expansions with null thickness stretching) or full Lagrange z-expansions, making progress on the application of high-order 2D plate models for analysis and design of advanced composite panels for aerospace applications. Therefore, it is possible to discuss and select the most suitable structural theories, capable of rendering numerically accurate and computationally efficient predictions, for supersonic panel flutter analysis of curvilinear fibre composites and its aeroelastic design optimization. To the best of the authors' knowledge, this is the first time that various ESL and LW 2D type finite elements, involving either the FSDT or TSDT displacement fields as well as full 3D displacements with Lagrange type z-expansions up to the third order, are compared specifically for panel flutter and buckling analysis of curvilinear fibre composite panels under supersonic airflow and uniaxial loads, providing a comparison with Rayleigh–Ritz CLPT solutions by Moreira et al. [32] whenever thin plates are considered. Hence, the present work allows the accuracy assessment of the FE models predictive capabilities as well as of the simpler and widely used Rayleigh–Ritz formulation with CLPT, in both flutter and buckling responses. The main novelties brought to light by this work regard the application of progressively refined multilayered plate models for the study of flutter and buckling characteristics in variable stiffness composite panels under supersonic airflow and uniaxial compressive loads, pushing forward the modelling predictive capabilities to quasi-3D descriptions, which have not yet been explored to such extent in the literature concerning the aeroelastic stability of the emerging and promising curvilinear fibre composites. Furthermore, the full non-linear Green–Lagrange strains and the von Kármán approximations are both investigated, whereas the First-order Piston Theory is assumed as aerodynamic model. Note that even though the proposed structural models correspond to particular cases that can be derived using the aforementioned unified formulations, a more conventional approach was adopted in the present formulation, but still in a fairly systematic manner. In line with the benchmark cases considered in static and free vibration analysis by Moreira et al. [22], as also followed in the Rayleigh–Ritz flutter analysis by Moreira et al. [32], numerical applications address not only three distinct curvilinear fibre composite laminates, but also a quite standard cross-ply configuration for comparison purposes. The assessment of the models predictive capabilities is focused on simply supported panels, providing a benchmark of flutter and buckling solutions for thin and moderately thick plates with various side-to-thickness ratios. Ultimately, the aeroelastic stability analysis of pre-stressed supersonic panels is presented, assuming solely the case of thin plates, which are indeed the ones of primary interest for aerospace applications, focusing on the evaluation of the combined flutter–buckling stability diagrams/maps.

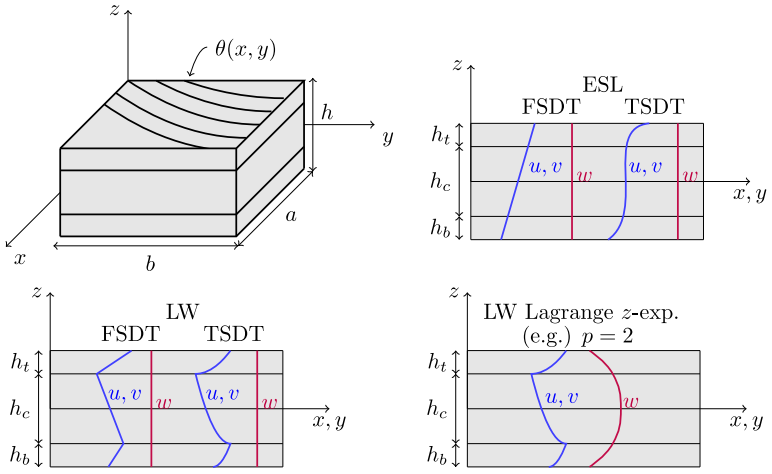

Fig. 1. Illustrative representation of a laminated composite panel with spatially varying fibre orientations, divided in three discrete layers: geometry and adopted structural models.

2. Structural models

In this work, both ESL and LW descriptions are considered for the development of the multilayered structural models, while assuming different displacement type axiomatic theories. On one hand, the ESL models are based on shear deformation theories, namely the FSDT and TSDT. On the other, the LW models include not only shear deformation theories, but also further refined theories involving Lagrange z-expansions of all displacement components, with a variable p-order, which can provide quasi-3D predictive capabilities in the sense that transverse normal deformations can be captured due to the non constant through-thickness distribution of transverse displacements, as illustrated in Fig. 1.

In agreement with linear elasticity, the models which account for transverse normal strains make use of 3D constitutive equations, given in the global coordinate system (x, y, z) as follows:

$$\begin{Bmatrix} \sigma_{xx} \\ \sigma_{yy} \\ \sigma_{zz} \\ \sigma_{yz} \\ \sigma_{xz} \\ \sigma_{xy} \end{Bmatrix} = \begin{bmatrix} \bar{C}_{11} & \bar{C}_{12} & \bar{C}_{13} & 0 & 0 & \bar{C}_{16} \\ \bar{C}_{12} & \bar{C}_{22} & \bar{C}_{23} & 0 & 0 & \bar{C}_{26} \\ \bar{C}_{13} & \bar{C}_{23} & \bar{C}_{33} & 0 & 0 & \bar{C}_{36} \\ 0 & 0 & 0 & \bar{C}_{44} & \bar{C}_{45} & 0 \\ 0 & 0 & 0 & \bar{C}_{45} & \bar{C}_{55} & 0 \\ \bar{C}_{16} & \bar{C}_{26} & \bar{C}_{36} & 0 & 0 & \bar{C}_{66} \end{bmatrix} \begin{Bmatrix} \epsilon_{xx} \\ \epsilon_{yy} \\ \epsilon_{zz} \\ \gamma_{yz} \\ \gamma_{xz} \\ \gamma_{xy} \end{Bmatrix} \tag{1}$$

where σ_{ij} represents the stresses, ϵ_{ii} the infinitesimal normal strains, γ_{ij} the engineering shear strains and $\bar{C}_{ij}$ the 3D elastic constants for layers involving pointwise orthotropic materials. In a more compact and convenient form, one has $\boldsymbol{\sigma} = \bar{\boldsymbol{C}}\boldsymbol{\epsilon}$, where $\boldsymbol{\sigma}$ and $\boldsymbol{\epsilon}$ are the stresses and strains structured as vectors (in line with Voigt notation), respectively.

However, in the typical approach to develop models that neglect transverse normal strains, as the ones that make use of shear deformation theories, it is assumed reduced plane stress constitutive equations ($\sigma_{zz} = 0$), given as shown:

$$\begin{Bmatrix} \sigma_{xx} \\ \sigma_{yy} \\ \sigma_{yz} \\ \sigma_{xz} \\ \sigma_{xy} \end{Bmatrix} = \begin{bmatrix} \bar{Q}_{11} & \bar{Q}_{12} & 0 & 0 & \bar{Q}_{16} \\ \bar{Q}_{12} & \bar{Q}_{22} & 0 & 0 & \bar{Q}_{26} \\ 0 & 0 & \bar{Q}_{44} & \bar{Q}_{45} & 0 \\ 0 & 0 & \bar{Q}_{45} & \bar{Q}_{55} & 0 \\ \bar{Q}_{16} & \bar{Q}_{26} & 0 & 0 & \bar{Q}_{66} \end{bmatrix} \begin{Bmatrix} \epsilon_{xx} \\ \epsilon_{yy} \\ \gamma_{yz} \\ \gamma_{xz} \\ \gamma_{xy} \end{Bmatrix} \tag{2}$$

where $\bar{Q}_{ij}$ are the reduced elastic constants (see Reddy [43] for further details on 3D and reduced constants). In compact form, one has $\boldsymbol{\sigma} = \bar{\boldsymbol{Q}}\boldsymbol{\epsilon}$.

In the particular case of curvilinear fibre composite layers, the fibre angle distribution is dependent on the in-plane coordinates in the general form of $\theta = \theta(x, y)$, which means that the elastic constants in the global coordinate system are continuously graded as well, i.e. $\bar{\boldsymbol{C}} = \bar{\boldsymbol{C}}(x, y)$, due to the necessary in-plane rotation between the layer material coordinate system and the global one [43]. In the present work, it is assumed that each composite layer has just a linear fibre angle variation along the x-axis, expressed as follows:

$$\theta(x) = T_0 + \frac{2(T_1 - T_0)}{a}\left|x - \frac{a}{2}\right|, \ 0 \le x \le a \tag{3}$$

where $T_0 = \theta(a/2)$ and $T_1 = \theta(0) = \theta(a)$ are the orientations at the centre and edges of the plate and a is the side along the x-axis (Fig. 1), respectively.

Under the assumption of infinitesimal strains, the geometrical strain–displacement relations correspond to the linear terms of the Green–Lagrange strain tensor, which are given by:

$$\epsilon_{xx} = u_{,x} \tag{4a}$$
$$\epsilon_{yy} = v_{,y} \tag{4b}$$
$$\epsilon_{zz} = w_{,z} \tag{4c}$$
$$\gamma_{yz} = v_{,z} + w_{,y} \tag{4d}$$
$$\gamma_{xz} = u_{,z} + w_{,x} \tag{4e}$$
$$\gamma_{xy} = u_{,y} + v_{,x} \tag{4f}$$

where u, v and w are the displacement components in the x-, y- and z-axis, respectively, such that the displacement vector is $\boldsymbol{u} = \{u\ v\ w\}^T$. The comma-derivative notation is adopted from now on.

Regarding the computation of the virtual work done by the applied in-plane loads in linear stability analysis, the non-linear terms of the Green–Lagrange in-plane strains are considered, as shown:

$$\tilde{\epsilon}_{xx} = \frac{1}{2}\left[\left(u_{,x}^2 + v_{,x}^2\right)\varpi + w_{,x}^2\right] \tag{5a}$$
$$\tilde{\epsilon}_{yy} = \frac{1}{2}\left[\left(u_{,y}^2 + v_{,y}^2\right)\varpi + w_{,y}^2\right] \tag{5b}$$
$$\tilde{\gamma}_{xy} = \left(u_{,x}u_{,y} + v_{,x}v_{,y}\right)\varpi + w_{,x}w_{,y} \tag{5c}$$

where ϖ is a scalar variable taking the value one or zero, thus allowing to adopt either the full non-linear in-plane strains or the well-known von Kármán strains, respectively. The generalized non-linear strain vector is conveniently written for later derivations as $\tilde{\boldsymbol{\epsilon}} = \{u_{,x}\ u_{,y}\ v_{,x}\ v_{,y}\ w_{,x}\ w_{,y}\}^T$.

2.1. ESL descriptions with no thickness stretching

In ESL descriptions, the independent variables of the kinematic model are introduced for the whole laminate, without depending on the number of material layers. Even though different kinematic models can be explored in ESL descriptions, as in the CUF [11], this work only considers shear deformation theories with no thickness stretching. In particular, the FSDT and TSDT make use of Taylor z-expansions of the

displacements around the mid-plane of the laminate, whose coefficients correspond to the independent variables of the theory. Assuming a constant through-thickness distribution of transverse displacements, sustained by the transverse inextensibility hypothesis, the FSDT and TSDT assume linear and cubic z-expansions of in-plane displacements, respectively. Specifically, the TSDT displacement field is given by:

$$u(x,y,z) = u_0(x,y) + z\theta_x(x,y) + z^2\beta_x(x,y) + z^3\lambda_x(x,y) \tag{6a}$$

$$v(x,y,z) = v_0(x,y) + z\theta_y(x,y) + z^2\beta_y(x,y) + z^3\lambda_y(x,y) \tag{6b}$$

$$w(x,y,z) = w_0(x,y) \tag{6c}$$

where the subscript 0 stands for the mid-plane location, θ_x and θ_y denote the rotations of the normals to the mid-plane about the y- and x-axes, respectively, whereas β_x, β_y, λ_x and λ_y are the higher-order generalized displacements. The displacement field of the FSDT is recovered by neglecting the high-order terms in the expansion of the in-plane displacements. In general, the nine degrees of freedom (DOFs) involved in the ESL TSDT are $\boldsymbol{d} = \{u_0\ v_0\ w_0\ \theta_x\ \theta_y\ \beta_x\ \beta_y\ \lambda_x\ \lambda_y\}^T$, whereas for the ESL FSDT, only the first five DOFs remain.

Since the FSDT predicts a just constant through-thickness distribution of shear strains, a shear correction factor K_s is applied for the evaluation of transverse shear stresses [43]. On the other hand, the TSDT predicts a more realist distribution of shear strains and, therefore, it does not require the introduction of a correction factor as the FSDT.

2.2. LW descriptions

Dividing a laminate into a set of discrete layers, which may correspond to the physical layers or to a given combination of layers (sub-laminates), LW descriptions treat each of them as an unique plate/shell, while imposing *a priori* the necessary continuity of displacements (and transverse stresses in mixed models) at the interfaces between adjacent layers [11]. As a result, LW descriptions are capable to predict through-thickness distributions of displacements with zig-zag behaviour, being especially suited for multilayered structures with high inhomogeneity of material properties through-thickness as well as thick panels. Moreover, various structural theories can be considered in view of the LW modelling, assuming either a prescribed or variable number of discrete layers *a priori*, as necessary. In the present work, both Lagrange z-expansions (of all displacement components) and shear deformation theories are included to obtain the LW displacements of a panel divided in three discrete layers, as presented in Fig. 1. The through-thickness continuity of transverse stresses is not enforced in the proposed displacement based formulations, as a common procedure in this type of approach [12], since it would lead to cumbersome manipulations of the displacement field (then depending on the elastic coefficients of the material layers), with no significant improvement as far as the global response accuracy is considered, as regards to the case of vibration and flutter characteristics. In fact, this is corroborated further by the assessment of LW mixed models for free vibration analysis of thin and moderately thick composite plates [44].

Assuming the same p-order Lagrange expansion for each displacement component and for all discrete layers, the displacement field of the k-layer can be written as follows:

$$u^k(x,y,z) = \sum_{j=1}^{n_u} \varphi_j^k(z) u_j^k(x,y) \tag{7a}$$

$$v^k(x,y,z) = \sum_{j=1}^{n_u} \varphi_j^k(z) v_j^k(x,y) \tag{7b}$$

$$w^k(x,y,z) = \sum_{j=1}^{n_u} \varphi_j^k(z) w_j^k(x,y) \tag{7c}$$

where $n_u = p+1$ is the number of points, φ_j^k are the Lagrange functions of the k-discrete layer and u_j^k, v_j^k and w_j^k are the associated through-thickness displacement variables at the j-point.

The Lagrange functions, through each layer thickness, in terms of the natural coordinate $\zeta^k \in [-1,\ 1]$, are defined as shown:

$$\varphi_j^k\left(\zeta^k\right) = \prod_{\substack{s=1 \\ s\neq j}}^{n_u} \frac{\zeta^k - \zeta^{k_s}}{\zeta^{k_j} - \zeta^{k_s}} \tag{8}$$

where $\zeta^k = 2(z - z_0^k)/h^k$, denoting z_0^k and h_k as the mid-plane z-coordinate and thickness of the k-discrete layer, respectively.

Since Lagrange z-expansions allow the independent variables to correspond to displacements at prescribed locations, equidistant across each layer thickness, the interlaminar continuity of displacements can be easily achieved by assembling of the displacement variables at adjacent layers. Thus, for a LW description which makes use of p-order Lagrange thickness-expansions, the total number of DOFs depends on the number of discrete layers (N_L), which corresponds to $(N_L - 1)$ interfaces, each with three displacement components to be assembled, leading to $(N_L \times (p+1) - 3 \times (N_L - 1))$ independent variables.

Considering a set of three discrete layers, denoted by bottom (b), core (c) and top (t), as represented in Fig. 1, the through-thickness continuity of displacements implies that $\boldsymbol{u}_{n_u}^b = \boldsymbol{u}_1^c$ (bottom-core interface) and $\boldsymbol{u}_{n_u}^c = \boldsymbol{u}_1^t$ (core-top interface), where $\boldsymbol{u}_j^k = \{u_j^k\ v_j^k\ w_j^k\}^T$ is the displacement vector of the k-layer at the j-node. The assembled DOFs for a generic p-order expansion, with $n_u = p+1$ points, are $\boldsymbol{d} = \{\boldsymbol{u}_1^{bT}\ \boldsymbol{u}_2^{bT}\ \ldots\ \boldsymbol{u}_{n_u}^{bT}\ \boldsymbol{u}_2^{cT}\ \ldots\ \boldsymbol{u}_{n_u}^{cT}\ \boldsymbol{u}_2^{tT}\ \ldots\ \boldsymbol{u}_{n_u}^{tT}\}^T$.

On the other hand, it is also possible to obtain LW descriptions making use of the FSDT and TSDT displacements, for each discrete layer, as well as the through-thickness displacement continuity. For three-discrete layers, the LW FSDT and LW TSDT displacement fields can both be explicitly found in Moreira et al. [22] (or in Moreira et al. [45] in the case of the former model), being here omitted for brevity. Nonetheless, it is worth remarking that the total number of independent variables for three discrete layers is reduced to $3N-6$, where $N = 5$ and 9 for the piecewise FSDT and TSDT, respectively, when imposing the continuity of displacements at the interfaces between the mid-layer and the outer ones. Since the transverse displacement is constant in the thickness direction of each layer, it is also constant throughout the entire thickness of the laminate (thus no thickness stretching can be captured). As presented by Moreira et al. [32], the twenty one DOFs associated to LW TSDT for three discrete layers are $\boldsymbol{d} = \{u_0^c\ v_0^c\ w_0^c\ \theta_x^c\ \theta_y^c\ \beta_x^c\ \beta_y^c\ \lambda_x^c\ \lambda_y^c\ \theta_x^t\ \theta_y^t\ \beta_x^t\ \beta_y^t\ \lambda_x^t\ \lambda_y^t\ \theta_x^b\ \theta_y^b\ \beta_x^b\ \beta_y^b\ \lambda_x^b\ \lambda_y^b\}^T$, whereas for the LW FSDT, only nine DOFs remain, since the high-order generalized displacements are not included.

3. Aeroelastic FE equations

For briefness and conciseness, the FE formulation is presented resorting to a general notation involving matrices and vectors, whose components are dependent on the adopted structural theory. Hence, for a general k-discrete layer, the combined 1D thickness-expansions and 2D FE approximations of the displacement vector $\boldsymbol{u}^k$ and the strain vectors $\boldsymbol{\epsilon}^k$ and $\tilde{\boldsymbol{\epsilon}}^k$ (i.e., linear and generalized non-linear strain components, respectively) are defined by:

$$\boldsymbol{u}^k = \boldsymbol{Z}^k \boldsymbol{N}^k \boldsymbol{d} \tag{9a}$$

$$\boldsymbol{\epsilon}^k = \boldsymbol{S}^k \boldsymbol{B}^k \boldsymbol{d} \tag{9b}$$

$$\tilde{\boldsymbol{\epsilon}}^k = \tilde{\boldsymbol{S}}^k \tilde{\boldsymbol{B}}^k \boldsymbol{d} \tag{9c}$$

where $\boldsymbol{Z}^k$, $\boldsymbol{S}^k$ and $\tilde{\boldsymbol{S}}^k$ contain the expansion functions in the thickness direction, while $\boldsymbol{N}^k$, $\boldsymbol{B}^k$ and $\tilde{\boldsymbol{B}}^k$ establish the necessary FE approximations in-plane via 2D shape functions. To be more precise, for ESL models involving a unique discrete layer, the dependency on the index k does not apply. Additionally, the applied 2D shape functions are, in fact, quadratic Lagrange functions – which form the basis of the nine-node quadrilateral element [43], usually denoted by Q9 – such that the element DOFs associated to the intended structural model are $\boldsymbol{d} = \{\boldsymbol{d}_1^T\ \ldots\ \boldsymbol{d}_9^T\}^T$, where $\boldsymbol{d}_i$ stands for the element nodal DOFs.

The C^0-interpolation in-plane, required by the adopted structural FE models, is then verified by the 2D Lagrange polynomials [43], for both shear deformation theories and Lagrange z-expansion models, thus ensuring the interelement continuity of primary variables (as in a conforming element). The same 2D shape functions are also considered for the approximation of the geometry, resulting in an isoparametric FE formulation [43].

In line with the Principle of Hamilton, the dynamic equilibrium of the composite panel divided in k discrete layers of in-plane surface $S = [0, a] \times [0, b]$ and thickness domain h^k, under supersonic airflow – which exerts a transverse pressure Δp on the upper surface of the top layer ($z = h/2$ and $k = t$) – and applied in-plane stresses on the edges, can be expressed in the following form:

$$\sum_k \int_S \int_{h^k} \delta\boldsymbol{\varepsilon}^{k^T} \boldsymbol{\sigma}^k + \delta\tilde{\boldsymbol{\varepsilon}}^{k^T} \hat{\boldsymbol{\sigma}}_{\mathbf{0}}^k \tilde{\boldsymbol{\varepsilon}}^{k^T} + \rho^k \delta\boldsymbol{u}^{k^T} \ddot{\boldsymbol{u}}^k \, dz dS = \int_S \delta\boldsymbol{u}^{t^T} |_{\frac{h}{2}} \boldsymbol{e}_z \Delta p \, dS \tag{10}$$

where δ stands for the variational operator and the double-dot for the second time derivative, while ρ^k is the k-layer density and $\boldsymbol{e}_z = \{0\ 0\ 1\}^T$. To include the von Kármán approximations along with the full non-linear strains on the models formulation, in line with Eq. (5), the initial stresses acting on the k-layer are expressed as shown:

$$\hat{\boldsymbol{\sigma}}_{\mathbf{0}}^k = \begin{bmatrix} \varpi\boldsymbol{\sigma}_{\mathbf{0}}^k & 0 & 0 \\ 0 & \varpi\boldsymbol{\sigma}_{\mathbf{0}}^k & 0 \\ 0 & 0 & \boldsymbol{\sigma}_{\mathbf{0}}^k \end{bmatrix} \tag{11}$$

with

$$\boldsymbol{\sigma}_{\mathbf{0}}^k = \begin{bmatrix} \sigma_{xx_0}^k & \sigma_{xy_0}^k \\ \sigma_{xy_0}^k & \sigma_{yy_0}^k \end{bmatrix} \tag{12}$$

Depending on the intended problem, the initial stress state in Eq. (12) is prescribed using zeros or ones, followed by a pre-multiplier α, which means, for instance, in the case of uniaxial loads along the x-axis, that $\sigma_{xx_0}^k = \alpha$ and $\sigma_{yy_0}^k = \sigma_{xy_0}^k = 0$. The most significant stress resultants along the thickness, i.e the in-plane loads per unit length acting on the boundaries, are given by:

$$\{N_x \ N_y \ N_{xy}\}^T = \sum_k \int_{h^k} \left\{\sigma_{xx_0}^k \ \sigma_{yy_0}^k \ \sigma_{xy_0}^k\right\}^T dz \tag{13}$$

Additionally, the effect of the supersonic airflow is described making use of the well-established First-order Piston Theory [27,40,46], which describes the pressure distribution acting on the upper surface of the panel as follows:

$$\Delta p = -\lambda \left(w_{,x} \cos\Lambda + w_{,y} \sin\Lambda\right) |_{\frac{h}{2}} - \mu\dot{w}|_{\frac{h}{2}} \tag{14}$$

where the dynamic pressure parameter and aerodynamic damping are given by $\lambda = 2q_\infty/(M_\infty^2 - 1)^{1/2}$ and $\mu = \lambda[(M_\infty^2 - 2)/(M_\infty^2 - 1)]/U_\infty$, respectively, denoting $q_\infty = \rho_\infty U_\infty^2/2$, ρ_∞, U_∞ and M_∞ as the dynamic pressure, density, speed and Mach number of the free airflow. Moreover, Λ represents the yaw angle of the airflow. In particular, the contribution of the aerodynamic damping is neglected since its inclusion leads to slightly higher critical flutter speeds [37]. Hence, more conservative flutter analyses can be ensured when imposing $\mu = 0$ in Eq. (14), as also followed by Moreira et al. [32].

Introducing the FE approximations stated in Eq. (9), the constitutive relations in Eqs. (1) or (2) as well as the aerodynamic pressure distribution in Eq. (14), all together, into in Eq. (10), one can derive the equilibrium equations of the element (for different kinematic models). In the end, the aeroelastic equilibrium equations accounting for in-plane loads are written as follows:

$$\boldsymbol{M}\ddot{\boldsymbol{d}} + (\boldsymbol{K} + \lambda\boldsymbol{K}_{\boldsymbol{a}} + \alpha\boldsymbol{K}_{\boldsymbol{g}})\boldsymbol{d} = \mathbf{0} \tag{15}$$

where $\boldsymbol{M}$ is the mass matrix, $\boldsymbol{K}$ the (purely elastic) stiffness matrix, $\lambda\boldsymbol{K}_{\boldsymbol{a}}$ the aerodynamic stiffness matrix and $\alpha\boldsymbol{K}_{\boldsymbol{g}}$ the geometric stiffness matrix. As derived from the variational formulation, the element matrices are given by:

$$\boldsymbol{M} = \sum_k \int_\Omega \boldsymbol{N}^{k^T} \left(\int_{h^k} \rho^k \boldsymbol{Z}^{k^T} \boldsymbol{Z}^k dz\right) \boldsymbol{N}^k d\Omega \tag{16a}$$

$$\boldsymbol{K} = \sum_k \int_\Omega \boldsymbol{B}^{k^T} \left(\int_{h^k} \boldsymbol{S}^{k^T} \bar{\boldsymbol{C}}^k \boldsymbol{S}^k dz\right) \boldsymbol{B}^k d\Omega \tag{16b}$$

$$\boldsymbol{K}_{\boldsymbol{g}} = \sum_k \int_\Omega \tilde{\boldsymbol{B}}^{k^T} \left(\int_{h^k} \tilde{\boldsymbol{S}}^{k^T} \hat{\boldsymbol{\sigma}}_{\mathbf{0}}^k \tilde{\boldsymbol{S}}^k dz\right) \tilde{\boldsymbol{B}}^k d\Omega \tag{16c}$$

$$\boldsymbol{K}_{\boldsymbol{a}} = \int_\Omega \boldsymbol{N}^{t^T} \boldsymbol{Z}^{t^T} |_{\frac{h}{2}} \boldsymbol{e}_z \boldsymbol{e}_z^T \boldsymbol{Z}^t |_{\frac{h}{2}} \left(\boldsymbol{N}_{,x}^t \cos\Lambda + \boldsymbol{N}_{,y}^t \sin\Lambda\right) d\Omega \tag{16d}$$

where the $\bar{\boldsymbol{C}}^k$ tensor is replaced by $\bar{\boldsymbol{Q}}^k$ whenever shear deformation models are considered (since they make use of reduced constitutive equations). In addition, the integrals in the thickness direction are obtained using analytical integration, whereas the integration on the in-plane FE domain Ω is carried out numerically, using Gauss quadrature, with reduced integration for the shear terms of the stiffness matrix (Eq. (16b)) in order to avoid shear locking in thin plates [43]. It is worth remarking that: (i) for curvilinear fibre composite layers, the fibre angle is evaluated at each integration point within an element and (ii) if a discrete layer represents more than one physical layer, this sublaminate is then treated as an ESL and, therefore, the integrals in the thickness direction must account for the sum of the different layers. Also noteworthy is that even when neglecting both structural and aerodynamic dissipative terms in the aeroelastic equilibrium equations, one needs to account for complex eigenvalue solutions since the aerodynamic stiffness matrix is non-symmetric (thus adding aeroelastic coupling between the vibration modes).

After proceeding with the FE assemblage and the application of boundary conditions, the global eigenvalue problem associated to Eq. (15) is written as shown:

$$\left|\left(\boldsymbol{K} + \lambda\boldsymbol{K}_{\boldsymbol{a}} + \alpha\boldsymbol{K}_{\boldsymbol{g}}\right) - s_n\boldsymbol{M}\right| = \mathbf{0} \tag{17}$$

where the complex eigenvalue of the n-mode is defined by $s_n = \omega_n^2(1 + ig_n)$, with $i = \sqrt{-1}$. For aeroelastic flutter analysis without in-plane loads, the pre-load multiplier is $\alpha = 0$ and, in contrast, for a pure buckling analysis in vacuum, the dynamic pressure parameter is $\lambda = 0$ and the inertial terms are also neglected. The particular case of free vibration in vacuum is obtained with $\lambda = \alpha = 0$ and $s_n = \omega_n^2$. Thus, the solution of the eigenvalue problem yields the natural frequencies (ω_n) and damping loss factors (g_n) in flutter analysis (for a given load level and dynamic pressure parameter), as well as the critical load parameter (α_{cr}) in buckling analysis. In short, as the dynamic pressure parameter increases, flutter occurs when the damping factor of one mode turns from positive to negative and, therefore, the system becomes dynamically unstable above the critical flutter dynamic pressure parameter λ_F. Actually, in the absence of any dissipative terms, all modes show a zero damping factor before flutter and mode coalescence flutter occurs [32], i.e. the eigenvalues of the modes involved in flutter emerge as complex conjugated pairs after the flutter bound and the associated natural frequencies coalesce to the same value, as carefully illustrated in the numerical applications.

4. Numerical applications

As intended in this work, the accuracy assessment of the developed FE models in supersonic panel flutter and buckling analysis is presented for both straight and curvilinear fibre composites, considering simply supported square panels with various side-to-thickness ratios. In more detail, the test cases are based on previous studies on static and free vibration analysis of variable stiffness composite laminates by Moreira et al. [22]. As a result, this work extends the previous FE benchmark solutions for the case of panel flutter and buckling analysis by considering the same three-layer composite laminates, with linear fibre angle variations $\langle T_0, T_1 \rangle$ along the x-axis as given in Eq. (3). Additionally, the flutter and buckling FE solutions of thin panels are also compared with

Rayleigh–Ritz solutions reported, in part, by Moreira et al. [32], which makes use of the CLPT, assuming solely bending deformations and sinusoidal type expansions of the mid-plane transverse displacement to fulfil the essential boundary conditions.

The complete stacking sequences of the symmetric laminates are as follows:

- *Constant stiffness composite (CSC)*: (0/90/0)
- *Variable stiffness composite 1 (VSC1)*: (⟨0, 45⟩/⟨-45, -60⟩/⟨0, 45⟩)
- *Variable stiffness composite 2 (VSC2)*: (⟨30, 0⟩/⟨45, 90⟩/⟨30, 0⟩)
- *Variable stiffness composite 3 (VSC3)*: (⟨90, 45⟩/⟨60, 30⟩/⟨90, 45⟩)

In terms of geometry, the square panels have side $a = b = 1$ m and a total thickness h depending on the side-to-thickness ratio $a/h = 250$, 100, 50 and 20, i.e. from thin to moderately thick plates. The composite layers have equal thickness ($h/3$) and are made of graphite–epoxy material with the following mechanical properties: $E_1 = 173$ GPa, $E_2 = E_3 = 7.20$ GPa, $G_{12} = G_{13} = G_{23} = 3.76$ GPa, $\nu_{12} = \nu_{13} = \nu_{23} = 0.29$ and $\rho = 1540$ kg/m^3. It is worth noting that even though moderately thick panels may not be of primary interest for most aeronautical and aerospace applications, especially when considering conventional metallic structures, they are also included for two reasons: (i) considering that composite panels can be more thick without compromising as much the structural weight and (ii) to further analyse the effect of shear deformation and transverse normal deformations on the aeroelastic response behaviour, which can only be predicted by refined structural models.

The aeroelastic analyses are carried out for airflow along the x-axis, i.e. normal flow with $\Lambda = 0°$, which is the same direction of the fibre angle variations. Likewise, the buckling analyses are solely presented for in-plane loads along the x-axis. The associated flutter dynamic pressure parameters and buckling loads are provided in the following nondimensionalized form:

$$\tilde{\lambda}_F = \frac{\lambda_F a^3}{h^3 G_{12}} \tag{18a}$$

$$\tilde{N}_{cr} = \frac{N_{cr} b^2}{h^3 E_2} \tag{18b}$$

All nondimensionalized flutter dynamic pressure parameters are estimated with a tolerance of $\Delta\tilde{\lambda} = 0.01$, which means that for $\tilde{\lambda} = \tilde{\lambda}_F - \Delta\tilde{\lambda}$, the frequencies of the modes involved in flutter have not already merged and all modes are dynamically stable, whereas for $\tilde{\lambda} = \tilde{\lambda}_F$, mode coalescence is present and the system becomes dynamically unstable due to the negative damping exhibited by one of the coalesced modes.

Furthermore, aeroelastic panel flutter analyses of pre-stressed thin panels are also presented, assuming uniaxial compressive loads along the airflow direction (i.e., the x-axis) as well as simply supported boundary conditions. The combined flutter–buckling stability diagrams/maps (flutter dynamic pressure parameter vs. in-plane load) are illustrated, comparing FE solutions with Rayleigh–Ritz CLPT solutions, while highlighting the operational regions where the panels remain both aeroelastically and statically stable.

To be clear, the simply supported boundary conditions are described by the following constraints:

$$u^k = w^k = 0 \quad \text{at } y = 0, b \tag{19a}$$

$$v^k = w^k = 0 \quad \text{at } x = 0, a \tag{19b}$$

where k stands for the different discrete layers. Depending on the structural theory of the FE model, different DOFs must be restrained to fulfil Eq. (19).

An additional remark may be relevant, at this point, concerning the fact that the Rayleigh–Ritz flutter solutions here presented are based on the work by Moreira et al. [32], which includes explicitly the case of panels with $a/h = 250$, although for $a/h = 100$, further Rayleigh–Ritz solutions are provided in the interest of the present work (thus here made available for the first-time). Likewise, buckling and flutter solutions of thin panels under uniaxial loads are made available for the first-time as well. Since in-plane loads are not contemplated in the original formulation presented by Moreira et al. [32], it is mentioned herein that the modal aeroelastic equilibrium equations for pre-stressed panels present a similar form to Eq. (15), however, the FE DOFs are replaced by the modal coordinates $\boldsymbol{q}$. The only matrix that is not presented explicitly in [32] is the modal geometric stiffness matrix, which is obtained in light of the von Kármán non-linear strains as shown:

$$\boldsymbol{K_g} = \int_0^a \int_0^b \begin{Bmatrix} \boldsymbol{\Psi}_{,x} \\ \boldsymbol{\Psi}_{,y} \end{Bmatrix}^T \begin{bmatrix} N_x^0 & N_{xy}^0 \\ N_{xy}^0 & N_y^0 \end{bmatrix} \begin{Bmatrix} \boldsymbol{\Psi}_{,x} \\ \boldsymbol{\Psi}_{,y} \end{Bmatrix} dy dx \tag{20}$$

where $\boldsymbol{\Psi}$ is the vector of sinusoidal trial functions, such that $w_0(x, y, t) = \boldsymbol{\Psi}^T(x, y)\boldsymbol{q}(t)$. In line with [32], six sinusoidal terms are applied in each in-plane direction for the expansion of the transverse displacement. The in-plane loads per unit length are given as stated in Eq. (13).

Regarding the adopted nomenclature for the structural models, whenever the LW reference does not appear on the name, it is assumed an ESL description. Besides, the models that make use of Lagrange z-expansions are denoted by LW Lag$p$, assuming expansions up to the third order ($p = 3$). To provide a complete assessment of the ESL FSDT predictive capabilities, two values of shear correction factor are considered: (i) an unitary value, i.e. $K_s = 1$, which means no shear correction (FSDT$^{(1)}$) and (ii) the usual $K_s = 5/6$ commonly found in the literature [43] (FSDT$^{(5/6)}$). In contrast, no shear correction is introduced in the LW FSDT and LW Lag1 formulations (as also followed in [22,45]). Furthermore, the Rayleigh–Ritz CLPT solutions are denoted by RR CLPT.

4.1. Convergence analysis: mesh refinement and non-linear strains

To ensure a proper selection of the FE mesh, Table 1 presents the convergence analysis results of the LW Lag3 model, considering the first three natural frequencies ω_n in vacuum, the nondimensionalized flutter dynamic pressure parameters $\tilde{\lambda}_F$ and flutter frequencies ω_F, as well as the nondimensionalized buckling loads $\tilde{N}_{cr}$ (along the x-axis) of the *CSC* and *VSC1* laminated panels with $a/h = 250$. The flutter frequency is defined as the value for which the natural frequencies involved in flutter coalesce together, namely the second and third modes for the *CSC* and the first and second modes for the *VSC1*. In addition, the FE buckling solutions given in Table 1 are obtained using the full non-linear Green–Lagrange strains, whereas the von Kármán strains are considered in the Rayleigh–Ritz solutions.

It is clearly perceived from Table 1 that the convergence of the free vibration, panel flutter and buckling solutions is much slower in the case of curvilinear fibre composites than for conventional straight fibre composites. As a result, the use of refined meshes appears necessary to accurately describe the in-plane stiffness distribution present in curvilinear fibre composites, even when accounting for fibre angle variations at each integration point (which, per se, is more advantageous for the convergence rate than assuming a just constant fibre orientation within each element). Since refined meshes require the use of more nodes and, consequently, more DOFs, it is quite crucial that the structural theory inherent to the FE ensures the best compromise between numerical accuracy and computational efficiency.

The discrepancy between Rayleigh–Ritz and FE solutions is also greater for the of case curvilinear fibre composites as discussed later on. Increasing the number of elements, both natural frequencies and buckling loads tend to decrease, whereas flutter dynamic pressures may increase or decrease. For the (0/90/0) composite laminate, one observes increasing flutter dynamic pressures, while the opposite occurs for the *VSC1*. Although not shown, for brevity, the remaining structural models show a similar convergence behaviour. Therefore, to ensure converged free vibration, buckling and flutter solutions, all together, either for straight or curvilinear fibre composites, a mesh with 14 × 14 Q9 elements is used in the models accuracy assessment presented hereafter.

Table 1
Convergence analysis results of the LW Lag3 model considering free vibration, flutter and buckling of thin panels with $a/h = 250$: *CSC* and *VSC1* laminates (ω in Hz).

Mesh Q9	DOFs	*CSC* (0/90/0)						*VSC1* ($\langle 0,45\rangle/\langle -45,-60\rangle/\langle 0,45\rangle$)					
		ω_1	ω_2	ω_3	$\tilde{\lambda}_F$	ω_F	$\tilde{N}_{cr}$	ω_1	ω_2	ω_3	$\tilde{\lambda}_F$	ω_F	$\tilde{N}_{cr}$
4 × 4	2430	20.682	31.492	57.551	1301.42	63.191	22.8605	23.155	38.252	63.656	551.73	39.176	27.3061
6 × 6	5070	20.670	31.331	55.662	1304.63	63.376	22.8425	22.982	37.831	61.818	547.33	39.141	26.7894
8 × 8	8670	20.667	31.303	55.316	1305.75	63.426	22.8394	22.907	37.707	61.463	546.34	39.106	26.5704
10 × 10	13230	20.667	31.295	55.217	1306.10	63.442	22.8385	22.862	37.647	61.354	545.93	39.077	26.4432
12 × 12	18750	20.667	31.292	55.181	1306.24	63.447	22.8382	22.832	37.610	61.310	545.69	39.055	26.3579
14 × 14	25230	20.667	31.291	55.165	1306.31	63.450	22.8380	22.809	37.584	61.288	545.55	39.039	26.2959
RR CLPT	36	20.673	31.298	55.169	1307.48	63.461	22.8536	24.030	39.783	63.694	619.98	41.910	29.6340

Table 2
Nondimensionalized buckling loads $\tilde{N}_{cr}$ of the *CSC* and *VSC1* laminates, with $a/h = 250$ and 20: comparison of von Kármán (*vK*) and Green–Lagrange (*GL*) non-linear strains.

Case	Model	$a/h = 250$		$a/h = 20$	
		vK	*GL*	*vK*	*GL*
CSC	FSDT[(1)]	22.8410	22.8404	21.0316	20.9537
	FSDT[(5/6)]	22.8384	22.8378	20.7037	20.6285
	TSDT	22.8386	22.8380	20.7292	20.6539
	LW FSDT	22.8399	22.8393	20.8969	20.8202
	LW TSDT	22.8386	22.8380	20.7228	20.6474
	LW Lag1	22.8850	22.8844	20.9299	20.8532
	LW Lag2	22.8387	22.8381	20.7308	20.6554
	LW Lag3	22.8386	22.8380	20.7303	20.6540
VSC1	FSDT[(1)]	26.3131	26.3120	23.7990	23.6557
	FSDT[(5/6)]	26.3084	26.3073	23.3760	23.2377
	TSDT	26.3028	26.3017	23.2864	23.1486
	LW FSDT	26.2972	26.2961	23.3951	23.2551
	LW TSDT	26.2855	26.2844	23.1140	22.9761
	LW Lag1	26.3724	26.3713	23.4664	23.3269
	LW Lag2	26.3037	26.3025	23.2085	23.0711
	LW Lag3	26.2970	26.2959	23.1438	23.0063

Furthermore, Table 2 presents a comparison of the von Kármán strains to the full non-linear strains on the evaluation of buckling loads, considering various structural theories as well as both straight and curvilinear fibre composite panels, with either $a/h = 250$ or 20. The use of full Green–Lagrange strains provides lower buckling loads than the von Kármán approximation, especially for moderately thick plates. Nonetheless, it is worth noting that the discrepancy between the two approaches is higher for the variable stiffness configuration, when comparing panels with the same side-to-thickness ratio. Therefore, the full non-linear strains are applied whenever in-plane loads are considered in further FE analyses, ensuring the most accurate solutions for both curvilinear fibre configurations and moderately thick panels.

4.2. Panel flutter and buckling analysis

The accuracy assessment of the proposed FE models in panel flutter and uniaxial buckling analysis is presented in Table 3, considering thin and moderately thick panels, as well as the four distinct composite laminates previously described, under supersonic airflow or applied in-plane loads along the x-axis. For each test case and each model, the presented aeroelastic results include the nondimensionalized flutter dynamic pressure parameter and the associated flutter frequency of the panel without in-plane loads applied.

It is firstly pointed out that regardless of the side-to-thickness ratio, flutter occurs with the coalescence of the second and third modes for the *CSC* cross-ply laminate, as well as the first and second modes for the *VSC1* and *VSC3* laminates. In contrast, for the *VSC2* laminate, flutters occurs due to the coupling of high-order modes, namely the fifth and sixth modes if $a/h = 250$, 100 and 50, as well as the sixth and seventh modes if $a/h = 20$. Actually, for the *VSC1* and *VSC2* laminates, with $a/h = 100$, the evolution of the natural frequencies and damping factors with the dynamic pressure parameter, predicted by the LW FSDT and LW Lag3 models, is provided in Fig. 2. A close examination of Fig. 2 reveals that as the natural frequencies coalesce, the eigenvalues of the modes involved in flutter emerge as complex conjugated pairs, with one of the modes exhibiting negative damping. As a result, the system becomes dynamically unstable and flutter appears. For the *VSC1*, it is clearly perceived that flutter occurs indeed due to the coalescence of the lowest two natural frequencies, while the remaining frequencies are not much influenced by the airflow. On the other hand, for the *VSC2*, flutter occurs on the fifth and sixth natural frequencies, even though a later coalescence of the first two can be identified for higher values of dynamic pressure. Fig. 2 also shows that for both laminates, the trends predicted by the two models are in good agreement.

To provide a more complete understanding and comparison of the response behaviour of the different laminates, Fig. 3 shows the buckling and flutter modes of thin panels with $a/h = 100$. Noticeable differences can be found in terms of both buckling and flutter in-plane mode shapes when comparing the straight fibre composite to the curvilinear fibre configurations, which came to light due to the distinct stiffness distributions in-plane, induced by the curvilinear fibres, as well as due to the different modes involved in the occurrence of flutter. Regarding the buckling response, the *VSC3* laminate is the only test case that shows a buckling mode with two peaks, whereas the remaining laminates feature a buckling mode with just a single peak. The flutter modes are illustrated for $\lambda = \lambda_F$, neglecting in-plane external loads. It is worth remarking that the flutter absolute maximum transverse displacement of the cross-ply composite laminate occurs at $x/a = 0.75$, whereas for the variable stiffness configurations, it can move either slightly forward or backward. Additionally, in the case of curvilinear fibre composites, the flutter modes are not symmetric with respect to $y/b = 0.5$. The flutter in-plane mode shape of the *VSC2* laminate, represented in Fig. 3, has indeed the most complicated spatial distribution since it occurs with the coalescence of high-order modes, as shown in Fig. 2.

For the cross-ply thin panels, one concludes from Table 3 that the Rayleigh–Ritz CLPT solutions are in good agreement with the FE predictions, having a discrepancy to the most refined model (LW Lag3) of 0.01% and 0.1% in terms of flutter pressure parameter when considering $a/h = 250$ and 100, respectively. However, for composite panels with curvilinear fibres, the discrepancies between the Rayleigh–Ritz and the FE flutter solutions increase significantly, assuming values from 5% to 16% depending on the fibre orientations and side-to-thickness ratio of the panel. Likewise, the Rayleigh–Ritz and FE buckling solutions are in good agreement with each other for the cross-ply laminate (discrepancy less than 1% when considering the LW Lag3 model as reference), but for the variable stiffness configurations, the discrepancies vary from 1% to 13% depending on the laminate. Taking the *VSC2* laminate as an example, the Rayleigh–Ritz model estimates buckling loads 1% and 1.5% higher than the LW Lag3 solutions for panels with $a/h = 250$ and 100, respectively. However, for the *VSC1* and *VSC3*, the discrepancy goes up to 13% and 11%, respectively, either for $a/h = 250$ or 100. Despite the fact that the CLPT neglects shear deformations, leading to higher flutter dynamic pressures and buckling loads, one must note that the accuracy of the Rayleigh–Ritz solutions is also influenced by the chosen trial functions. In line with the conclusions outlined by Stone and Chandler [33], the in-plane expansion of the transverse displacement in terms of sinusoidal functions tends to overpredict the stiffness of composite laminates with high flexural

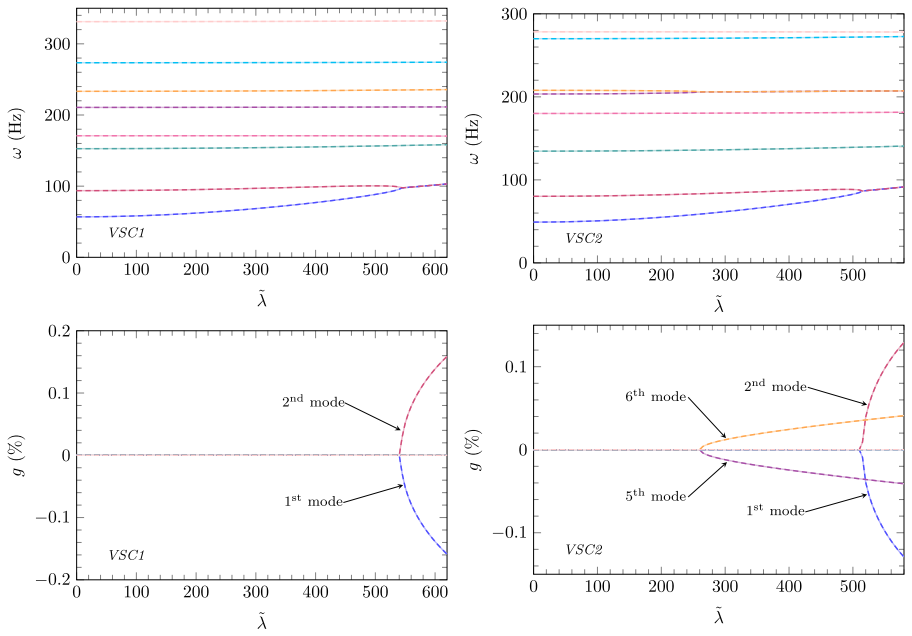

Fig. 2. Variation of the first eight natural frequencies ω_n and damping factors g_n with the nondimensionalized dynamic pressure parameter $\tilde{\lambda}$ of the *VSC1* and *VSC2* laminate panels, with $a/h = 100$, predicted by the LW Lag3 model (solid lines) and by the LW FSDT model (dashed lines).

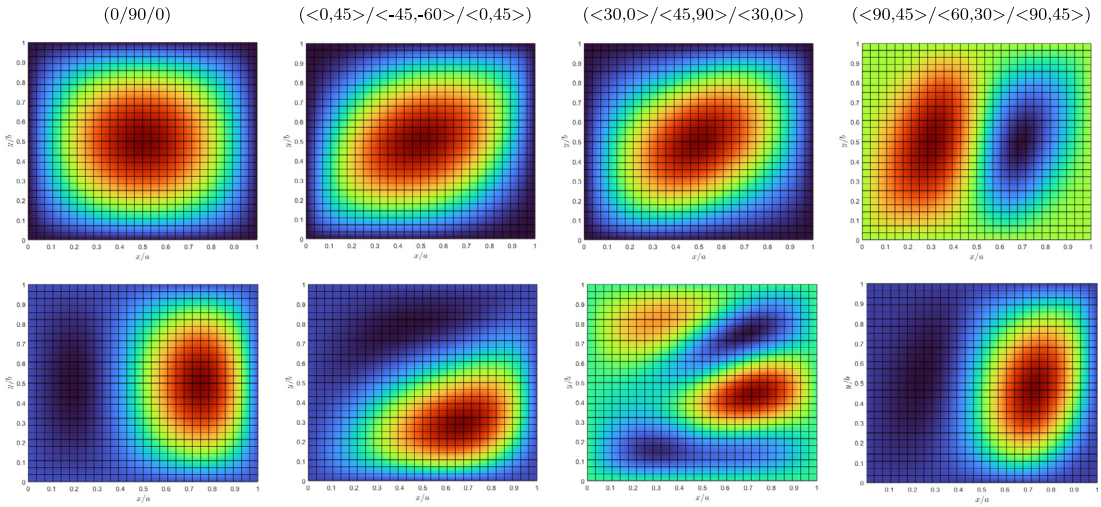

Fig. 3. Buckling and flutter in-plane mode shapes $w(x, y, 0)$ – first and second lines, respectively – of thin panels with $a/h = 100$, predicted by the LW Lag3 model.

anisotropy, involving bending–twisting coupling, such as the curvilinear fibre composites investigated herein. Ergo, as far as curvilinear fibre composite laminates are considered, it is concluded that even for thin panels, the Rayleigh–Ritz CLPT formulation using sinusoidal expansions provides a rather deficient estimation for panel flutter and buckling analysis, leading to higher flutter pressure parameters, flutter frequencies and buckling loads.

As the side-to-thickness ratio decreases, differences between the first- and high-order models begin to appear, both in terms of flutter dynamic pressure parameters and buckling loads. Regarding the FE models that make use of ESL descriptions, one can perceive from Table 3 that the shear correction has a significant impact on the accuracy of the FSDT in comparison to the TSDT. In particular, the FSDT solutions with $K_s = 5/6$ are in good agreement with the TSDT solutions, being slightly lower or higher depending on the laminate (e.g., for the *CSC* and *VSC2*, the FSDT with $K_s = 5/6$ underestimates the flutter dynamic pressures in comparison to the TSDT model, whereas for the *VSC1* and *VSC3* they are overestimated). On the other hand, the FSDT model with $K_s = 1$ yields overestimated predictions when compared to the application of $K_s = 5/6$ or a high-order theory. Since the accuracy of the (ESL) FSDT depends strongly on the proper selection of the shear correction factor – which is influenced not only by the geometry and boundary conditions, but also by the in-plane distribution of fibre orientations – higher-order modelling may be preferable within ESL descriptions to obtain accurate panel flutter and buckling solutions in variable stiffness composite laminates, without the introduction of problem-dependent shear correction factors.

Between the two LW approaches without thickness stretching, the piecewise cubic model predicts lower flutter dynamic pressure parameters and buckling loads for all laminates and side-to-thickness ratios due to the higher flexibility that the LW TSDT allows, in each layer thickness, namely in terms of transverse shear deformations. Nevertheless, both models are in good agreement with the ESL TSDT model, which has the same number of DOFs as the LW FSDT, but less than half of the LW TSDT. Hence, it is highlighted that as far as first-order models are considered, the LW modelling is preferable to the ESL modelling due to a lower impact of the non-introduction of a shear correction factor on the accuracy of the flutter and buckling solutions. In other

Table 3
Nondimensionalized flutter pressure parameters $\tilde{\lambda}_F$, flutter frequencies ω_F (Hz) and nondimensionalized buckling loads $\tilde{N}_{cr}$ of simply supported composite panels, with various side-to-thickness ratios.

Case	Model	$a/h = 250$			$a/h = 100$			$a/h = 50$			$a/h = 20$		
		$\tilde{\lambda}_F$	ω_F	$\tilde{N}_{cr}$	$\tilde{\lambda}_F$	ω_F	$\tilde{N}_{cr}$	$\tilde{\lambda}_F$	ω_F	$\tilde{N}_{cr}$	$\tilde{\lambda}_F$	ω_F	$\tilde{N}_{cr}$
CSC	RR CLPT	1307.48	63.461	22.854	1307.25	158.622	22.854	–	–	–	–	–	–
	FSDT$^{(1)}$	1306.64	63.457	22.840	1296.40	158.185	22.771	1261.52	313.255	22.525	1072.39	740.720	20.954
	FSDT$^{(5/6)}$	1306.26	63.450	22.838	1294.05	158.085	22.755	1252.83	312.516	22.464	1038.26	733.392	20.629
	TSDT	1306.29	63.451	22.838	1294.26	158.093	22.756	1253.60	312.574	22.468	1040.40	733.321	20.654
	LW FSDT	1306.49	63.453	22.839	1295.51	158.146	22.764	1258.20	312.968	22.500	1058.73	737.537	20.820
	LW TSDT	1306.29	63.451	22.838	1294.24	158.092	22.756	1253.52	312.568	22.467	1040.17	733.311	20.647
	LW Lag1	1307.68	63.486	22.884	1296.76	158.217	22.809	1259.90	313.092	22.544	1071.35	741.386	20.853
	LW Lag2	1306.31	63.450	22.838	1294.39	158.084	22.756	1254.32	312.540	22.470	1052.90	737.002	20.655
	LW Lag3	1306.31	63.450	22.838	1294.37	158.083	22.756	1254.25	312.534	22.468	1052.73	737.028	20.654
VSC1	RR CLPT	619.98	41.910	29.634	619.72	104.743	29.634	–	–	–	–	–	–
	FSDT$^{(1)}$	545.55	39.042	26.312	543.28	97.489	26.193	535.44	194.195	25.817	488.46	473.240	23.656
	FSDT$^{(5/6)}$	545.47	39.041	26.307	542.80	97.469	26.168	533.62	194.044	25.728	479.84	471.293	23.238
	TSDT	545.45	39.039	26.302	542.51	97.436	26.154	532.84	193.884	25.697	477.18	469.896	23.149
	LW FSDT	545.38	39.033	26.296	542.38	97.401	26.146	532.89	193.768	25.701	478.85	469.530	23.255
	LW TSDT	545.34	39.030	26.284	541.92	97.356	26.112	531.41	193.539	25.617	473.45	467.730	22.976
	LW Lag1	548.42	39.142	26.371	545.44	97.669	26.223	535.99	194.267	25.779	482.91	470.617	23.327
	LW Lag2	545.58	39.042	26.303	542.36	97.400	26.142	532.31	193.654	25.666	476.71	468.288	23.071
	LW Lag3	545.55	39.039	26.296	542.17	97.373	26.125	531.77	193.527	25.634	475.21	467.470	23.006
VSC2	RR CLPT	302.21	83.665	19.821	304.52	209.078	19.821	–	–	–	–	–	–
	FSDT$^{(1)}$	289.20	82.889	19.599	265.23	206.205	19.539	180.64	405.440	19.330	358.08	927.646	18.011
	FSDT$^{(5/6)}$	288.20	82.875	19.597	259.02	205.984	19.526	156.12	403.802	19.278	454.66	425.183	17.746
	TSDT	288.46	82.874	19.597	260.65	205.975	19.526	162.75	403.730	19.280	443.90	916.593	17.757
	LW FSDT	289.11	82.881	19.598	264.72	206.077	19.533	178.77	404.481	19.306	362.15	918.018	17.890
	LW TSDT	288.60	82.873	19.597	261.55	205.962	19.526	166.32	403.630	19.279	421.98	913.996	17.753
	LW Lag1	269.20	83.057	19.658	244.36	206.520	19.592	156.38	405.404	19.365	402.79	922.837	17.943
	LW Lag2	288.60	82.879	19.599	261.19	205.992	19.528	164.18	403.807	19.283	443.49	917.051	17.766
	LW Lag3	288.65	82.879	19.599	261.54	205.985	19.528	165.56	403.748	19.283	435.77	915.879	17.765
VSC3	RR CLPT	182.34	33.314	15.564	182.26	83.266	15.564	–	–	–	–	–	–
	FSDT$^{(1)}$	169.88	31.592	14.033	169.20	78.805	13.972	166.98	156.501	13.775	153.97	374.878	12.641
	FSDT$^{(5/6)}$	169.86	31.557	14.031	169.06	78.770	13.959	166.47	156.251	13.732	151.65	371.874	12.443
	TSDT	169.85	31.589	14.030	169.03	78.766	13.958	166.38	156.232	13.726	151.22	371.661	12.418
	LW FSDT	169.85	31.589	14.031	169.06	78.778	13.961	166.54	156.329	13.742	152.04	372.919	12.497
	LW TSDT	169.82	31.586	14.028	168.95	78.752	13.953	166.20	156.172	13.716	150.75	371.256	12.392
	LW Lag1	171.15	31.673	14.125	170.36	78.982	14.056	167.83	156.706	13.837	153.48	373.533	12.592
	LW Lag2	169.88	31.593	14.034	169.05	78.770	13.961	166.36	156.190	13.731	151.39	371.141	12.432
	LW Lag3	169.87	31.592	14.034	169.01	78.763	13.959	166.28	156.163	13.726	151.14	370.929	12.419

words, the LW FSDT does not rely upon the careful selection of shear corrections factors as much as the ESL FSDT. For TSDT models, the ESL modelling ensures a better compromise between numerical accuracy and computational efficiency than the LW modelling as far as composite laminates are considered (i.e. excluding sandwich panels with high through-thickness inhomogeneity of material properties).

As regards to the LW models which account for thickness stretching, it is firstly remarked that the LW Lag1 solutions are highly impacted by thickness locking and, therefore, this model provides higher flutter dynamic pressures, frequencies and buckling loads than the remaining FE models (the only exception is in the flutter dynamic pressure parameters of the *VSC2*, which are severely underpredicted). More specifically, the thickness locking effect, also known as Poisson locking, arises by the application of simplified kinematic assumptions in the analysis of plates/shells (namely constant transverse normal strains in the layers thickness direction) and is significantly dependent in the inherent coupling between out-of-plane and in-plane normal strains in the 3D constitutive law presented in Eq. (1). Even though some techniques can be found in the literature to avoid thickness locking in first-order models with either linear or constant through-thickness distributions of the transverse displacement, as discussed in detail by Carrera and Brischetto [47], they are not considered in this work because ESL and LW models making use of shear deformation theories and plane stress constitutive equations are presented instead. To be precise, apart from assuming a high-order kinematic description for the transverse displacement, the use of reduced plane stress constitutive equations is indeed one of the suggested techniques to mitigate thickness locking in theories with constant transverse normal strains [47].

As one increases the Lagrange z-expansion order above two, the flutter and buckling predictions begin to converge and it is pointed out that thickness locking does vanish when considering high-order modelling, as expected. Hence, the LW Lag2 is already capable of properly capturing most of the in-plane and transverse deformations involved in both mechanical phenomena, as compared to the further refined LW Lag3. Nonetheless, the major discrepancies between the LW Lag2 and LW Lag3 models appear for moderately thick plates, especially when the flutter analysis of curvilinear fibre composites is considered due to both transverse shear deformations and bending–twisting coupling being strongly intrinsic to such panel configurations featuring aeroelastic coupling. Actually, the highest discrepancy between the two high-order Lagrange models in the prediction of buckling loads is just 0.3% (found for the *VSC2* laminate, with $a/h = 20$).

Comparing the LW Lag3 model to the LW TSDT model, i.e. the layerwise cubic models with and without thickness stretching, respectively, it is concluded that the latter tends to predict slightly lower flutter pressure parameters and buckling loads for most of the laminates and side-to-thickness ratios. The exception is the *VSC2* laminate when considering panels with $a/h = 100$ and 50, where the LW TSDT predicts higher flutter dynamic pressures than the LW Lag3, however, the discrepancy is lower than 0.5%. Additionally, when analysing the *VSC2* laminate in the form of a moderately thick panel with $a/h = 20$, the LW TSDT underestimates the flutter pressure in 3.2% with respect to the LW Lag3, which is noted as the highest discrepancy between the LW TSDT and LW Lag3 models, and the only case where the discrepancy between these models is higher than 1%. These discrepancies can be justified by the fact the LW TSDT makes use of plane stress constitutive

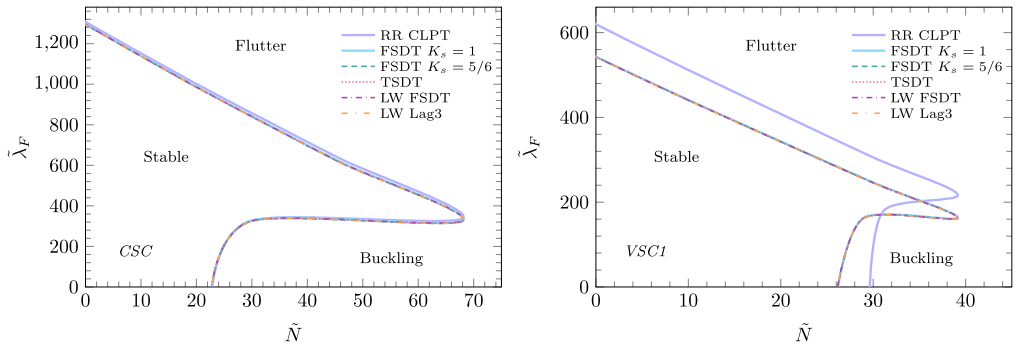

Fig. 4. Variation of the nondimensionalized flutter dynamic pressure parameter $\tilde{\lambda}_F$ with the uniaxial compressive load $\tilde{N}$, considering thin panels with $a/h = 100$ and various structural models: *CSC* (on the left) and *VSC1* (on the right).

equations and neglects transverse normal deformations, so that the (transverse) aerodynamic pressure and the in-plane compressive loads are both applied with respect to the mid-plane transverse displacement, which is assumed to have constant through-thickness distribution. On the contrary, the Lagrange z-expansion theories allow the aerodynamic load to be applied at the very top surface of the panel, while accounting for transverse normal strains and stresses along the thickness.

In fact, among the presented test cases, the highest discrepancies between the different structural theories in terms of the predicted flutter pressure parameters are found for the *VSC2* laminate, in which flutter occurs with the coalescence of high-order modes, as opposed to the remaining laminates where flutter appears among the first three modes. Considering the *VSC2* laminate, the (absolute) discrepancies in flutter dynamic pressure between the FSDT based models and the LW Lag3 model are around 1% for panels with $a/h = 100$, whereas high-order models (either ESL or LW) are much closer. As one moves to panels with $a/h = 50$, the mean discrepancy between the first-order models and the most refined model (LW Lag3) is around 8%, while for the ESL TSDT, the discrepancy is just 2%. Actually, for $a/h = 50$, only the LW TSDT and the LW Lag2 predict flutter dynamic pressures with a discrepancy less than 1% to the LW Lag3. To conclude the detailed analysis of the *VSC2* laminate, it is worth noting that for $a/h = 20$, the accuracy of the ESL FSDT model is compromised by the two adopted values of shear correction factor. Specifically, for $K_s = 1$, the flutter dynamic pressure is 18% lower than the one predicted by the LW Lag3 model, while for $K_s = 5/6$ it is 4% higher. However, in the latter, flutter emerges from the coalescence of the first two modes as opposed to the sixth and seventh modes, which results in a completely distinct flutter frequency. Similarly, the LW FSDT with $K_s = 1$ is not very accurate for panels with $a/h = 20$, having an absolute discrepancy of 17% to the LW Lag3 model, since for moderately thick plates, the contributions of both transverse shear deformations and transverse normal stretching to the overall strain energy increase significantly with respect to the case of thin panels. Hence, in the case of $a/h = 20$, the high-order models are indeed the ones that provide solutions with a discrepancy lower than 4%, where the closest model to the LW Lag3 is the LW Lag2, with 1.8% of discrepancy, because this model retains both through-thickness linear transverse shear deformations and transverse normal strains. Nonetheless, there is still quite a noticeable improvement when considering the case of transverse strains with through-thickness quadratic distributions, which are attainable through cubic expansions of the displacements, as in the LW Lag3.

4.3. Panel flutter analysis under uniaxial loads

The final assessment consists on the aeroelastic flutter analysis of pre-stressed panels, under supersonic airflow and in-plane compressive loads parallel to the x-axis. For brevity, only thin panels with $a/h = 100$ are considered in this final assessment and the *VSC3* is not investigated.

Table 4
Nondimensionalized flutter dynamic pressure parameters $\tilde{\lambda}_F$ of thin panels with $a/h = 100$, under supersonic airflow and uniaxial compressive loads $\tilde{N}$ along the x-axis.

Case	Model	$\tilde{N} = 0$	$\delta(\%)^a$	$\tilde{N} = 1$	$\delta(\%)^a$	$\tilde{N} = 10$	$\delta(\%)^a$
CSC	RR CLPT	1307.25	1.00	1291.58	1.02	1152.44	1.30
	FSDT$^{(1)}$	1296.40	0.16	1280.55	0.16	1139.93	0.20
	FSDT$^{(5/6)}$	1294.05	−0.02	1278.17	−0.03	1137.31	−0.03
	TSDT	1294.26	−0.01	1278.39	−0.01	1137.55	−0.01
	LW FSDT	1295.51	0.09	1279.65	0.09	1138.94	0.11
	LW TSDT	1294.24	−0.01	1278.37	−0.01	1137.53	−0.01
	LW Lag2	1294.39	0.002	1278.52	0.002	1137.69	0.002
	LW Lag3	1294.37	–	1278.50	–	1137.67	–
VSC1	RR CLPT	619.72	14.30	608.82	14.47	511.79	16.31
	FSDT$^{(1)}$	543.28	0.20	532.96	0.21	441.19	0.26
	FSDT$^{(5/6)}$	542.80	0.12	532.46	0.11	440.60	0.13
	TSDT	542.51	0.06	532.18	0.06	440.32	0.06
	LW FSDT	542.38	0.04	532.05	0.04	440.27	0.05
	LW TSDT	541.92	−0.05	531.59	−0.05	439.78	−0.06
	LW Lag2	542.36	0.04	532.04	0.04	440.22	0.04
	LW Lag3	542.17	–	531.85	–	440.04	–
VSC2	RR CLPT	304.52	16.43	289.95	17.22	174.29	26.24
	FSDT$^{(1)}$	265.23	1.41	251.15	1.54	142.79	3.43
	FSDT$^{(5/6)}$	259.02	−0.96	244.87	−1.00	135.99	−1.50
	TSDT	260.65	−0.34	246.49	−0.35	137.45	−0.44
	LW FSDT	264.72	1.22	250.58	1.31	141.71	2.64
	LW TSDT	261.55	0.004	247.38	0.01	138.24	0.13
	LW Lag2	261.19	−0.13	247.01	−0.14	137.76	−0.22
	LW Lag3	261.54	–	247.35	–	138.06	–

[a] $\delta(\%) = \left(\tilde{\lambda}_F - \tilde{\lambda}_F^{\text{LW Lag3}}\right) \times 100/\tilde{\lambda}_F^{\text{LW Lag3}}$.

In fact, thin panels are the ones of primary interest for most aeronautical and aerospace applications and the ratio $a/h = 100$ defines, in particular, the assumed limit of validity of the CLPT [43]. Likewise, the LW Lag1 model is not considered since it consistently leads to overestimated predictions when compared to the remaining models.

Table 4 presents the nondimensionalized dynamic pressure parameters obtained with the different models for various load levels, which are nondimensionalized according to $\tilde{N} = N_x^0 b^2/(E_2 h^3)$, where N_x^0 is the applied compressive load per unit length. It is worth remarking that all load levels considered in the numerical assessment shown in Table 4, viz. $\tilde{N} = 1$ and 10, are below the critical buckling load (see Table 3) and do not influence the modes involved in flutter, which are identified in the previous subsection for $\tilde{N} = 0$. For higher load levels, the aeroelastic flutter results are illustrated in Fig. 4, which shows the predicted stability diagrams of the *CSC* and *VSC1* laminates.

According to Table 4 and Fig. 4, for the (0/90/0) *CSC* laminate, the Rayleigh–Ritz CLPT model predicts slightly higher flutter dynamic pressures than the FE models. To be precise, for low load levels (say $\tilde{N} \leq 10$), the discrepancy is around 1%, while for higher loads it can go up to 4%. Therefore, the Rayleigh–Ritz and FE solutions can be

considered in good agreement with each other from a purely practical point of view, as also perceived by the quasi-superposed lines shown in Fig. 4.

As consistently demonstrated thus far, the Rayleigh–Ritz CLPT solutions overestimate the overall stiffness of composite panels with high flexural anisotropy, involving bending–twisting coupling, leading to higher buckling loads and flutter dynamic pressures than those obtained using the developed FE models. However, the discrepancies increase considerably when comparing unloaded to pre-stressed curvilinear fibre composite panels, as concluded from Table 4, reaching values between 14% and 34% depending on the load level (Fig. 4). This is mainly explained by the fact that when the panels are under combined aerodynamic transverse loads and in-plane compressive stresses, the 3D mechanical response turns out to be more complicated, featuring bending, membrane and shear deformations, all together, which are even more challenging to be captured in highly anisotropic variable stiffness composites with spatially varying fibre orientations. Thus, the present Rayleigh–Ritz CLPT solutions, which assume a sinusoidal type expansion of the transverse displacement, are not considered sufficiently accurate in the case of pre-stressed curvilinear fibre composites, as opposed to the previous case concerning the cross-ply laminate. Carefully tailored structural modelling emerges quite crucial to properly evaluate the coupled aeroelastic-buckling response behaviour of such complex multilayered composites, accounting for transverse shear deformation as well as an accurate description of intricate in-plane stiffness distributions and elastic coupling effects.

For the *VSC1* laminate, the LW FSDT model predicts lower flutter dynamic pressures than the ESL FSDT model, when using $K_s = 1$ (as in the other test cases), but also for $K_s = 5/6$. Moreover, the LW FSDT model also predicts lower flutter dynamic pressures than the ESL TSDT model, as opposed to the remaining laminates. Resorting to LW modelling and increasing the z-expansion order of the displacements above two, especially in terms of in-plane components, one starts to obtain converged flutter solutions.

Additionally, the *VSC2* laminate shows the higher discrepancies between the Rayleigh–Ritz and FE solutions, as well as among the present set of FE models, since flutter occurs due to the coupling of high-order modes, namely the fifth and sixth ones. Taking the LW Lag3 solutions as reference, both the FSDT ($K_s = 1$) and LW FSDT overestimate the flutter dynamic pressure by more than 1%, whereas the FSDT ($K_s = 5/6$) underestimates it by 1% (thus highlighting an accurate prediction, which is particularly influence in FSDT models by the adopted shear correction factor). Additionally, the ESL TSDT model also underestimates the flutter resistance in comparison to LW Lag3 model, however, the discrepancy is just around 0.3%. The LW TSDT and LW Lag3 solutions are in good agreement, being slightly higher than the LW Lag2 solutions. As concluded by comparing the different composite laminates, the accuracy of the kinematic models is influenced by the fibre orientations and the resulting stiffness distribution (which is always characterized by flexural anisotropy, involving bending–twisting coupling, whenever curvilinear fibre composites are considered).

Comparing the models with and without transverse normal deformations, it is concluded that the inclusion of thickness stretching does not affect the aeroelastic flutter solutions of pre-stressed thin panels in the same magnitude as the refined modelling of the transverse shear deformation does. To be clear, this is indeed due to the fact that in the response of thin plates, the contribution of the transverse normal strain energy is relatively small when compared to other contributions regarding membrane and transverse shear deformations and, most especially, bending deformations. This is corroborated further by noting that there are no discrepancies in the transverse normal compressibility of the layers across the thickness of the panels, as opposed to what is usually found in soft core sandwich panels reinforced by stiff face layers (which possess a rather significant face-to-core stiffness ratio). Ultimately, high-order shear deformation models, even when based on ESL descriptions, can match the purpose of accurately predicting both in-plane deformations as well as transverse shear, without depending on the introduction of a shear correction factor as first-order models do.

5. Conclusions

In light of the increasing interest in exploring the exceptional tailorability of curvilinear fibre composites for design optimization of advanced aerospace structures, in which numerically accurate and computationally efficient aeroelastic models are crucial, this work provides an assessment of structural theories for aeroelastic flutter and buckling stability analysis of supersonic multilayered panels with spatially varying fibre orientations. The main novelties addressed by the present work regard the exploration of 2D type multilayered FE models involving both ESL and LW descriptions – with variable order and different type of through-thickness z-expansions of the displacements, either including or neglecting transverse normal deformations – for the evaluation of flutter and buckling characteristics in variable stiffness composite panels under supersonic airflow and uniaxial compressive loads. In fact, the proposed kinematic models are progressively refined to render quasi-3D predictive capabilities, which have not yet been explored to such extent in the literature, thus making progress on the study and application of the proper structural modelling for aeroelastic stability analysis of curvilinear fibre composites.

The models accuracy assessment is carried out for simply supported panels, assuming both thin and moderately thick plates. As far as thin panels are considered, the FE predictions are compared with Rayleigh–Ritz CLPT solutions, which is one of the most classical and widely used approaches for supersonic panel flutter analysis. All things considered, the numerical results lead to the following concluding remarks:

- For thin cross-ply laminates, the Rayleigh–Ritz CLPT solutions with sinusoidal type expansion, are in good agreement with the present FE predictions, showing a maximum discrepancy around 1% and 0.5% in terms of flutter bounds and buckling loads, respectively, despite the fact that all FE models account for transverse shear deformations, as opposed to the CLPT. However, for curvilinear fibre composites, the Rayleigh–Ritz solutions are rather deficient on account of the fibres orientations. Overall, it is highlighted that this Rayleigh–Ritz approach overestimates the bending stiffness of curvilinear fibre composite laminates, predicting flutter pressure parameters and buckling loads which can be 10% (or more) higher than those obtained using the proposed FE models.
- The introduction of curvilinear fibres adds not only challenges from the point of view of modelling the in-plane stiffness distribution and the inherent elastic coupling effects (e.g. bending–twisting), but also in the evaluation of transverse shear deformations. In fact, transverse shear plays a significant role on the flutter behaviour of moderately thick panels, which is even more pronounced when dealing with curvilinear fibres composites.
- As far as the flutter and buckling analysis of thin panels is considered, the use of LW descriptions does not improve significantly the ESL modelling when high-order shear deformation theories are applied or, instead, a first-order theory accompanied by a carefully selected shear correction factor;
- Thickness stretching can be neglected in thin panels, either with straight or curvilinear fibres, but its inclusion may be relevant as one considers moderately thick plates.
- The aeroelastic flutter response of pre-stressed panels is more influenced by the modelling of in-plane and transverse shear deformations than the case without external loading, especially when considering curvilinear fibre composites. Therefore, high-order theories, even when based on ESL descriptions, can match this purpose without depending on the introduction of a shear correction factor. In addition, Rayleigh–Ritz CLPT solutions involving sinusoidal type expansions may be suitable for the combined aeroelastic flutter–buckling stability analysis of thin cross-ply laminates, but not for curvilinear fibre configurations, since such estimations are rather deficient when compared to the presented FE predictions.

Ultimately, the accurate prediction of both elastic coupling effects and transverse shear deformations is highlighted as an important aspect to consider for proper tailoring and analysis of supersonic curvilinear fibre composite laminates under in-plane loads, underlying the need for refined structural models. Nevertheless, it is worth remarking that for soft core sandwich panels and smart laminates with surface-bonded piezoelectric patches/layers – which show a higher inhomogeneity of material properties through-thickness than the composite laminates investigated herein – some of the reported conclusions may not hold (equally true), namely when comparing the ESL and LW descriptions. Therefore, further ensuing research is focused on supersonic flutter and buckling analysis of advanced sandwich panels to ensure the selection of numerically accurate and computationally efficient structural models, suitable for aeroelastic control and design optimization applications. The assessment and comparison of ESL and LW models in the evaluation of the dynamic response of stresses is also an important aspect to consider in ensuing works, especially with focus on fatigue and failure predictions in the non-linear post-flutter regime.

CRediT authorship contribution statement

J.A. Moreira: Writing – review & editing, Writing – original draft, Visualization, Validation, Software, Resources, Methodology, Investigation, Funding acquisition, Formal analysis, Data curation, Conceptualization. **F. Moleiro:** Writing – review & editing, Supervision, Project administration, Methodology, Funding acquisition, Conceptualization. **A.L. Araújo:** Writing – review & editing, Supervision, Methodology, Funding acquisition, Conceptualization. **A. Pagani:** Writing – review & editing, Supervision, Funding acquisition, Conceptualization.

Declaration of competing interest

The authors declare that they have no known competing financial interests or personal relationships that could have appeared to influence the work reported in this paper.

Data availability

Data will be made available on request.

Acknowledgements

This work has been supported by National Funds through Fundação para a Ciência e a Tecnologia (FCT), Portugal, through IDMEC, under LAETA, project UIDB/50022/2020. J.A. Moreira appreciates the financial support of FCT, Portugal through the Ph.D. Grant 2021.06113.BD. In addition, A. Pagani acknowledges funding from the European Research Council (ERC) under the European Union's Horizon 2020 research and innovation programme (Grant agreement No. 850437).

References

[1] P. Ribeiro, H. Akhavan, A. Teter, J. Warmiński, A review on the mechanical behaviour of curvilinear fibre composite laminated panels, J. Compos. Mater. 48 (22) (2014) 2761–2777, http://dx.doi.org/10.1177/0021998313502066.

[2] C.S. Lopes, Z. Gürdal, P.P. Camanho, Variable-stiffness composite panels: Buckling and first-ply failure improvements over straight-fibre laminates, Comput. Struct. 86 (9) (2008) 897–907, http://dx.doi.org/10.1016/j.compstruc.2007.04.016.

[3] C.S. Lopes, Z. Gürdal, P.P. Camanho, Tailoring for strength of composite steered-fibre panels with cutouts, Composites A 41 (12) (2010) 1760–1767, http://dx.doi.org/10.1016/j.compositesa.2010.08.011.

[4] X. Ma, F. Wang, H. Wang, P. Hao, B. Wang, Post-buckling optimization of bending-induced variable stiffness composite cylinders considering worst geometric imperfections, Thin-Walled Struct. 169 (2021) 108489, http://dx.doi.org/10.1016/j.tws.2021.108489.

[5] H. Haddadpour, Z. Zamani, Curvilinear fiber optimization tools for aeroelastic design of composite wings, J. Fluids Struct. 33 (2012) 180–190, http://dx.doi.org/10.1016/j.jfluidstructs.2012.05.008.

[6] O. Stodieck, J.E. Cooper, P.M. Weaver, P. Kealy, Improved aeroelastic tailoring using tow-steered composites, Compos. Struct. 106 (2013) 703–715, http://dx.doi.org/10.1016/j.compstruct.2013.07.023.

[7] Z. Wang, D. Peeters, R. De Breuker, An aeroelastic optimisation framework for manufacturable variable stiffness composite wings including critical gust loads, Struct. Multidiscip. Optim. 65 (10) (2022) 290, http://dx.doi.org/10.1007/s00158-022-03375-x.

[8] T.A. Guimarães, S.G. Castro, C.E. Cesnik, D.A. Rade, Supersonic flutter and buckling optimization of tow-steered composite plates, AIAA J. 57 (1) (2019) 397–407, http://dx.doi.org/10.2514/1.J057282.

[9] J. Fazilati, V. Khalafi, Aeroelastic panel flutter optimization of tow-steered variable stiffness composite laminated plates using isogeometric analysis, J. Reinf. Plast. Compos. 38 (19–20) (2019) 885–895, http://dx.doi.org/10.1177/0731684419854800.

[10] J. Fazilati, V. Khalafi, Panel flutter analysis of perforated plate repaired by VSCL bonded patch using the multi-patch IGA approach, Thin-Walled Struct. 169 (2021) 108465, http://dx.doi.org/10.1016/j.tws.2021.108465.

[11] E. Carrera, Theories and finite elements for multilayered anisotropic, composite plates and shells, Arch. Comput. Methods Eng. 9 (2) (2002) 87–140, http://dx.doi.org/10.1007/BF02736649.

[12] K.M. Liew, Z.Z. Pan, L.W. Zhang, An overview of layerwise theories for composite laminates and structures: Development, numerical implementation and application, Compos. Struct. 216 (2019) 240–259, http://dx.doi.org/10.1016/j.compstruct.2019.02.074.

[13] F. Moleiro, C.M. Mota Soares, E. Carrera, J.N. Reddy, Evaluation of exact electro-elastic static and free vibration solutions of multilayered plates for benchmarking: piezoelectric composite laminates and soft core sandwich plates, Compos. Part C: Open Access 2 (2020) 100038, http://dx.doi.org/10.1016/j.jcomc.2020.100038.

[14] L. Demasi, G. Biagini, F. Vannucci, E. Santarpia, R. Cavallaro, Equivalent single layer, Zig-Zag, and layer wise theories for variable angle tow composites based on the generalized unified formulation, Compos. Struct. 177 (2017) 54–79, http://dx.doi.org/10.1016/j.compstruct.2017.06.033.

[15] A.R. Sánchez-Majano, R. Azzara, A. Pagani, E. Carrera, Accurate stress analysis of variable angle tow shells by high-order equivalent-single-layer and layer-wise finite element models, Materials 14 (21) (2021) http://dx.doi.org/10.3390/ma14216486, https://www.mdpi.com/1996-1944/14/21/6486.

[16] A. Viglietti, E. Zappino, E. Carrera, Analysis of variable angle tow composites structures using variable kinematic models, Composites B 171 (2019) 272–283, http://dx.doi.org/10.1016/j.compositesb.2019.03.072.

[17] Y. Yan, B. Liu, Y. Xing, E. Carrera, A. Pagani, Free vibration analysis of variable stiffness composite laminated beams and plates by novel hierarchical differential quadrature finite elements, Compos. Struct. 274 (2021) 114364, http://dx.doi.org/10.1016/j.compstruct.2021.114364.

[18] R. Vescovini, L. Dozio, A variable-kinematic model for variable stiffness plates: Vibration and buckling analysis, Compos. Struct. 142 (2016) 15–26, http://dx.doi.org/10.1016/j.compstruct.2016.01.068.

[19] A.R. Sánchez-Majano, A. Pagani, M. Petrolo, C. Zhang, Buckling sensitivity of tow-steered plates subjected to multiscale defects by high-order finite elements and polynomial chaos expansion, Materials 14 (11) (2021) http://dx.doi.org/10.3390/ma14112706, https://www.mdpi.com/1996-1944/14/11/2706.

[20] A. Pagani, A.R. Sánchez-Majano, Stochastic stress analysis and failure onset of variable angle tow laminates affected by spatial fibre variations, Compos. Part C: Open Access 4 (2021) 100091, http://dx.doi.org/10.1016/j.jcomc.2020.100091.

[21] A. Pagani, A.R. Sánchez-Majano, Influence of fiber misalignments on buckling performance of variable stiffness composites using layerwise models and random fields, Mech. Adv. Mater. Struct. 29 (3) (2022) 384–399, http://dx.doi.org/10.1080/15376494.2020.1771485.

[22] J.A. Moreira, F. Moleiro, A.L. Araújo, A. Pagani, Assessment of layerwise user-elements in Abaqus for static and free vibration analysis of variable stiffness composite laminates, Compos. Struct. 303 (2023) 116291, http://dx.doi.org/10.1016/j.compstruct.2022.116291.

[23] K. Mehar, S.K. Panda, Theoretical deflection analysis of multi-walled carbon nanotube reinforced sandwich panel and experimental verification, Composites B 167 (2019) 317–328, http://dx.doi.org/10.1016/j.compositesb.2018.12.058.

[24] A. Szekrényes, Application of differential quadrature method to delaminated first-order shear deformable composite plates, Thin-Walled Struct. 166 (2021) 108028, http://dx.doi.org/10.1016/j.tws.2021.108028.

[25] A. Szekrényes, Mechanics of shear and normal deformable doubly-curved delaminated sandwich shells with soft core, Compos. Struct. 258 (2021) 113196, http://dx.doi.org/10.1016/j.compstruct.2020.113196.

[26] P. Van Vinh, A. Tounsi, Free vibration analysis of functionally graded doubly curved nanoshells using nonlocal first-order shear deformation theory with variable nonlocal parameters, Thin-Walled Struct. 174 (2022) 109084, http://dx.doi.org/10.1016/j.tws.2022.109084.

[27] Y. Chai, W. Gao, B. Ankay, F.M. Li, C. Zhang, Aeroelastic analysis and flutter control of wings and panels: A review, Int. J. Mech. Syst. Dyn. 1 (1) (2021) 5–34, https://onlinelibrary.wiley.com/doi/abs/10.1002/msd2.12015.

[28] F.M. Li, Z.G. Song, Flutter and thermal buckling control for composite laminated panels in supersonic flow, J. Sound Vib. 332 (22) (2013) 5678–5695, http://dx.doi.org/10.1016/j.jsv.2013.05.032.

[29] Z.G. Song, F.M. Li, Aerothermoelastic analysis of lattice sandwich composite panels in supersonic airflow, Meccanica 51 (2013) 887–891, http://dx.doi.org/10.1007/s11012-015-0240-y.

[30] M. Rahmanian, M. Javadi, A unified algorithm for fully-coupled aeroelastic stability analysis of conical shells in yawed supersonic flow to identify the effect of boundary conditions, Thin-Walled Struct. 155 (2020) 106910, http://dx.doi.org/10.1016/j.tws.2020.106910.

[31] P. Li, Z. Yang, W. Tian, Nonlinear aeroelastic analysis and active flutter control of functionally graded piezoelectric material plate, Thin-Walled Struct. 183 (2023) 110323, http://dx.doi.org/10.1016/j.tws.2022.110323.

[32] J.A. Moreira, F. Moleiro, A.L. Araújo, A. Pagani, Analytical modeling of panel flutter and active control in supersonic variable stiffness composite laminates, Mech. Adv. Mater. Struct. (2022) 1–15, http://dx.doi.org/10.1080/15376494.2022.2144970.

[33] M.A. Stone, H.D. Chandler, Errors in double sine series solutions for simply supported symmetrically laminated plates, Int. J. Mech. Sci. 38 (5) (1996) 517–526, http://dx.doi.org/10.1016/0020-7403(95)00067-4.

[34] R. Vescovini, L. Dozio, M. D'Ottavio, O. Polit, On the application of the ritz method to free vibration and buckling analysis of highly anisotropic plates, Compos. Struct. 192 (2018) 460–474, http://dx.doi.org/10.1016/j.compstruct.2018.03.017.

[35] G. Sciascia, V. Oliveri, P.M. Weaver, Eigenfrequencies of prestressed variable stiffness composite shells, Compos. Struct. 270 (2021) 114019, http://dx.doi.org/10.1016/j.compstruct.2021.114019.

[36] G. Sciascia, V. Oliveri, P.M. Weaver, Dynamic analysis of prestressed variable stiffness composite shell structures, Thin-Walled Struct. 175 (2022) 109193, http://dx.doi.org/10.1016/j.tws.2022.109193.

[37] H. Akhavan, P. Ribeiro, Aeroelasticity of composite plates with curvilinear fibres in supersonic flow, Compos. Struct. 194 (2018) 335–344, http://dx.doi.org/10.1016/j.compstruct.2018.03.101.

[38] H. Akhavan, P. Ribeiro, Nonlinear flutter of composite laminates with curvilinear fibres using a full linearized aerodynamic theory, J. Fluids Struct. 115 (2022) 103756, http://dx.doi.org/10.1016/j.jfluidstructs.2022.103756.

[39] M. Rasool, M.K. Singha, Aeroelastic analysis of pre-stressed variable stiffness composite panels, J. Vib. Control 26 (9–10) (2020) 724–734, http://dx.doi.org/10.1177/1077546319889865.

[40] E. Carrera, E. Zappino, Aeroelastic analysis of pinched panels in supersonic flow changing with altitude, J. Spacecr. Rockets 51 (1) (2014) 187–199, http://dx.doi.org/10.2514/1.A32363.

[41] E. Zappino, E. Carrera, M. Cinefra, Aeroelastic analysis of composite pinched panels using higher-order shell elements, J. Spacecr. Rockets 52 (3) (2015) 999–1003, http://dx.doi.org/10.2514/1.A32986.

[42] Y. Yan, L. Zhang, Variable-kinematic finite elements for the aero-thermo-elastic analysis of variable stiffness composite laminates, Mech. Adv. Mater. Struct. (2022) 1–17, http://dx.doi.org/10.1080/15376494.2022.2119312.

[43] J.N. Reddy, Mechanics of Laminated Composite Plates and Shells – Theory and Analysis, second ed., CRC Press, Boca Raton, 2004.

[44] E. Carrera, An assessment of mixed and classical theories on global and local response of multilayered orthotropic plates, Compos. Struct. 50 (2) (2000) 183–198, http://dx.doi.org/10.1016/S0263-8223(00)00099-4.

[45] J.A. Moreira, F. Moleiro, A.L. Araújo, Layerwise electro-elastic user-elements in Abaqus for static and free vibration analysis of piezoelectric composite plates, Mech. Adv. Mater. Struct. 29 (21) (2022) 3109–3121, http://dx.doi.org/10.1080/15376494.2021.1886381.

[46] H. Ashley, G. Zartarian, Piston theory-a new aerodynamic tool for the aeroelastician, J. Aeronaut. Sci. 23 (12) (1956) 1109–1118, http://dx.doi.org/10.2514/8.3740.

[47] E. Carrera, S. Brischetto, Analysis of thickness locking in classical, refined and mixed multilayered plate theories, Compos. Struct. 82 (4) (2008) 549–562, http://dx.doi.org/10.1016/j.compstruct.2007.02.002.